Sea State Estimation with Neural Networks Based on the Motion of a Moored FPSO Subjected to Campos Basin Metocean Conditions

Gustavo A. Bisinotto(✉), Lucas P. Cotrim, Fabio Gagliardi Cozman, and Eduardo A. Tannuri

Escola Politécnica of University of São Paulo, São Paulo, Brazil
gustavo.bisinotto@usp.br

Abstract. Important information for the design and operation of oceanic systems can be obtained by assessing local sea state parameters such as significant height, peak period and incidence direction. Techniques for motion-based inference and their possible drawbacks have been extensively discussed in the literature (their motivation coming from the simplicity of the required instrumentation when compared to traditional measuring systems), and machine learning approaches are now appearing in a few investigations. This paper addresses the estimation problem through supervised learning, using time series with the movement of a moored vessel to train neural networks models so as to estimate the sea state. Such time series are obtained through simulations, that consider a model of a spread-moored FPSO (Floating Production Storage and Offloading) platform with constant draft, out of a set of metocean conditions observed at Brazil's Campos Basin. A sensitivity analysis for different classes of neural networks was run, based on the significant height estimation, to choose the network architecture with the best results with respect to the mean absolute error metric. That topology was trained and employed in the estimation of the remaining sea state parameter, separately. The outcomes of the proposed models were confronted with other neural networks-based methods and showed up a comparable or slightly better performance in the error metrics. A preliminary discussion of the ability of the approach to deal with some classical issues on motion-based estimation is presented.

Keywords: Sea state estimation · Neural networks · Moored FPSO · Metocean conditions

1 Introduction

The operation of ships and other oceanic structures, such as offshore platforms, is affected by loads induced by waves, wind and currents. Therefore, reliable ways to obtain information about those environmental effects provide essential

A. Britto and K. Valdivia Delgado (Eds.): BRACIS 2021, LNAI 13074, pp. 294–308, 2021.
https://doi.org/10.1007/978-3-030-91699-2_21

data for the design and engineering of installations, and they are also useful to support decision-making processes, assisting the crew in the evaluation of a particular operation, or in the need to interrupt it [17].

Over the last decades, wave measurement has been carried out mainly by moored wave-buoys, whose motions are measured so as to recover the conditions around the buoys (due to their negligible dynamics). However, the setup is prone to damage and loss, and suffers from deep water mooring setbacks [17].

Most marine vessels are equipped with sensors that gather vast amounts of data, such as inertial measuring units (IMU), accelerometers, anemometers. In this sense, those crafts are inherently equipped with sea state measuring systems, as their sensor data can be used to infer their on-site condition, similarly to what is done with traditional buoys [2].

When compared to other wave monitoring systems, estimation of sea state based on vessel's motions presents the main advantage of the simplicity of the required instrumentation (composed basically of accelerometers and rate-gyros), already available or easily installed on-board. On the other hand, the limitation is clear: only waves that impose a reasonable level of motion may be inferred, which means that the vessel acts as a low-pass filter, filtering the high-frequency components that do not excite its first-order response. The filter analogy also indicates that the range of frequencies where the estimation can be properly performed will depend on the size of the vessel. Large-displacement vessels, such as the Very Large Crude Carriers (VLCCs) on which the FPSO (Floating Production Storage and Offloading) units are usually based, will have lower cut-off frequencies if compared to smaller vessels [16].

During the past years, motion-based methods for wave inference have been widely studied, mainly focusing on the parametric and the Bayesian approaches.

The parametric method as applied to an FPSO platform can be found in Ref. [19]. The formulation considers the characterization of the directional wave spectrum by a set of parameters and a linear relation between the incident wave and the movements' spectra, which is modeled by the Response Amplitude Operators (RAOs). Thereafter, a nonlinear optimization problem can be defined to minimize the absolute difference between the measured spectra of motion and the one computed from crossing the RAOs and the parametrized wave spectrum.

The Bayesian approach can be found in Ref. [14], with application to a container ship with forward speed, and in Ref. [17] and Ref. [16], to a moored FPSO, among others, with a derivation that leads to a quadratic optimization problem. In this case the linearity assumption remains, but no closed-form is imposed on the wave spectrum. The estimation is performed by maximizing the product of the likelihood function by the prior distribution. The likelihood function represents the conditional probability of occurrence of a given measurement, given the directional spectrum, while the prior distribution corresponds to the previous information about the unknown spectrum coefficients.

Since then, variations have been made to the initial proposals, especially to the Bayesian method. For instance, take Ref. [4], with the analysis of the influence of the hyperparameters associated with the priors, along with a procedure

for their selection, and Ref. [5], with a combination of data from wave probes to the Bayesian modeling, to attenuate the effect of the filtering problem.

More recent years have seen machine learning-based proposals. For instance, in Ref. [1], where a Quadratic Discriminant Analysis classification and Least Square Regression were used to estimate the set of wave parameters and in [20] with the definition of a classification problem based on random forests.

Some other efforts based on neural networks can be found in the literature. In Ref. [6], time series of movements from an in-service frigate type vessel and data from numerical simulation were considered to output wave height, period and direction. In Ref. [3], a classification problem was analyzed with the definition of a sea state from discretized wave heights and directions adding up to a total of 40 possibilities, that were classified from zigzag motions of a research vessel.

From the previous discussion, it can be noticed that a large interest has been devoted to motion-based wave estimation methods in the last couple of decades, with several applications in simulations, experiments and field campaigns. However, few works have been yet carried out with machine learning techniques, particularly when taking into account large moored vessels such as FPSOs.

This paper aims to address sea state estimation from motions of a moored FPSO using neural networks. The motion data was obtained through simulations of the vessel subjected to a dataset of environmental conditions observed at Brazil's Campos Basin.

The next section presents an explanation of ocean waves and their parameters, where directional and power wave spectra are introduced, and also the sea state. This is followed by a brief discussion of different classes of neural networks in Sect. 3. The sea state estimation procedure is detailed in Sect. 4, with a description of the data and the process to select the architecture of the estimation model. In Sect. 5, the outcomes of the proposed method are displayed and discussed. Finally, some conclusions drawn from this study are presented along with possible further steps.

2 Background: the Description of Ocean Waves

There are two main types of waves affecting the behavior of oceanic structures: wind waves and swell. In both cases, the waves start as small ripples but increase in size due to the sustained energy from the wind. Wind waves result from the local wind blowing over a fetch of water, while a swell is created by winds that are no longer blowing; such waves are been generated elsewhere from a distance and are not significantly influenced by the local wind [12,15].

The most applied theory of waves in the dynamical analysis of marine systems is the linear wave theory, whose basic element is the linear regular wave [12]. Its dimensions associated with the propagation through space are depicted in Fig. 1. Besides those parameters, others that should be mentioned are the main direction of propagation and the wave period, which defines the time interval between the arrival of consecutive crests at a stationary point, and that can be associated with the wave length by a dispersion relation [13].

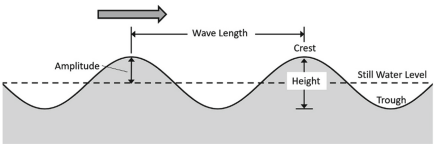

Fig. 1. Main space dimensions associated with linear regular waves [12]

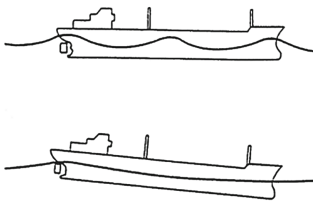

Fig. 2. Illustration of the filtering problem with a regular incident wave

The regular wave is also useful to illustrate the filtering problem on motion-based wave inference, as shown in Fig. 2. Where for low-frequency incident waves (on bottom) oscillatory motions are generated in the wave frequency (first-order response). While it can be noticed that for high-frequency waves (on top) the vessel is mostly not responsive to the wave excitation, and hence little movement is induced, making the estimation more challenging.

However, that description is not faithful to the actual ocean environment, as real ocean waves are irregular and random. Despite that, they can be modeled by a suitable distribution of regular waves. Under a linearity assumption, a superposition method can be applied, in which irregular waves can be described as the sum of regular components with different amplitudes and periods [12,13].

With this simplification, waves can be represented by a power spectrum, $S(\omega)$, that gives the distribution of energy among different frequencies, ω. To also account for the propagation of the components of the irregular wave in different directions, θ, the power spectrum can be extended to the directional spectrum, $S(\omega, \theta)$, that defines the distribution of energy over frequencies and directions. Examples of power and directional spectra are shown in Fig. 3.

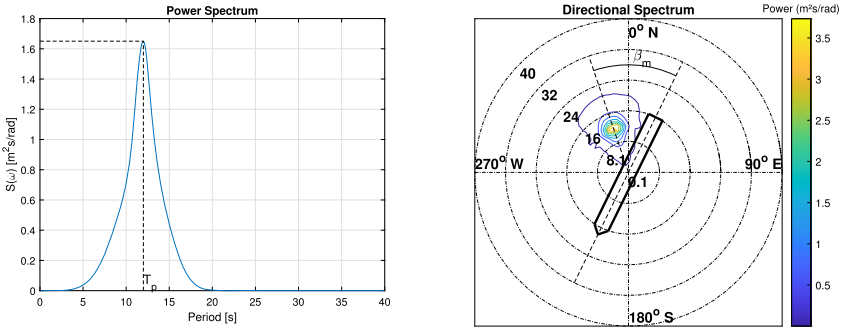

Fig. 3. Power and directional wave spectra

Due to the irregular nature of waves, it is not reasonable to assume a single wave height or wave period. Instead, wave statistics can be defined, such as

the significant wave height (H_s), that is computed as the average height of the highest one-third of the waves in the record, and the peak period (T_p), that is the period of maximum energy of the spectrum, among other possible characteristic periods [10]. From the analysis of the power spectrum, Fig. 3 (left), those parameters can be obtained as follows:

$$H_s = 4\sqrt{\int_0^\infty S(\omega)d\omega} \quad \text{and} \quad T_p = \frac{2\pi}{\omega_p}, \quad \omega_p = \underset{\omega}{\text{argmax}}\, S(\omega). \tag{1}$$

In the directional spectrum Fig. 3 (right), a contour plot is presented. Where the angular positions indicate the propagation direction, in degrees; the concentric lines correspond to periods, in seconds, of the wave components; and colors express the energy density of those components.

Because wind-generated waves are not uni-directional, an angular spread is adopted, thus defining a distribution of energy along the directions. Hence, two angular statistics can be defined to describe the wave propagation through space: the mean wave direction (β) and the relative wave direction (β_m). The mean wave incidence direction is usually measured clockwise from the vertical axis (from North), while the relative direction is a function of the incidence direction and the heading of the vessel ($\beta_{heading}$), depicted in Fig. 3 (right) and according to the following expression:

$$\beta_m = \pi + \beta_{heading} - \beta. \tag{2}$$

With the set of parameters (H_s, T_p, β) or (H_s, T_p, β_m), the sea state for a unimodal sea can be described. For multimodal seas, superposition can be applied with the individual wave spectra. And the sea state can be characterized by multiples sets of significant height, peak period and incidence direction.

3 Background: Neural Networks

Artificial Neural Networks (ANNs or simply NNs) essentially aim to approximate a function $y = f^*(x)$, that maps an input x to a continuous value or a categorical output y, defining a relation $y = f(x; \vartheta)$. From data, one must learn the value of the parameters ϑ that results in the best function approximation [7].

Convolutional neural networks (CNNs) are a particular class of neural networks specialized in processing data with a known grid-like topology. Those networks use multiple sets of shared weights, called filters, to respond to different patterns in the data. To this end, the general matrix multiplication between input and weights is replaced by a convolution operation in the formulation of the neurons [7].

The basic structure of a CNN [11] consists of a series of convolutional layers, with different depths and kernel dimensions, each associated with an activation function (usually nonlinear). And pooling layers that are responsible for reducing the size of the data by keeping local information of the mapping, such as maximum or average values. In this process, it is possible to extract features from

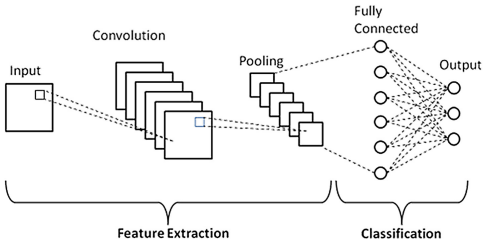

Fig. 4. CNN basic structure

the inputs by combining patterns underlined by each set of filters, which can be concatenated to feed an MLP for the final step of classification or regression.

Recurrent neural networks (RNNs) are a family of neural networks for sequential data processing, whose connections between layers model a dynamic temporal behavior for time-varying input series. However, traditional RNNs suffer from significant issues, the "vanishing or exploding gradients" effects, since it becomes difficult to backpropagate errors through a long-time span [7].

Long Short-Term Memory (LSTM) RNNs [9] deal with this problem by creating paths through time that have derivatives that neither vanish nor explode, with the application of a system of gating units to controls that data flow. In such a way that they can store information over extended time intervals.

4 An Estimation Procedure for Sea Parameters

The proposed estimation procedure was formulated as a supervised learning regression problem, where the goal is to compute each one of the sea state parameters (significant height, peak period and incidence direction) of a unimodal sea from time series of motion of a moored platform.

Fig. 5. FPSO platform at campos basin

Table 1. Information about the FPSO platform at campos basin

Quantity	Value
Vessel type	FPSO
Mooring	Spread-Moored
Length (L_{pp})	320 m
Breadth	54.5 m
Draft	16 m
Heading	206.16°

Those time series were obtained from simulations of the model in 6°C of freedom (dofs) of a typical spread-moored FPSO unit, Fig. 5, with one loading condition (single draft) under a dataset of metocean conditions that were observed at Brazil's Campos Basin.

For data generation, the simulation model, along with the platform information, Table 1, and the environmental conditions were considered as inputs to the Dynasim simulator, a hydro-dynamical numerical simulator developed by a partnership between the Numerical Offshore Tank Laboratory of the University of São Paulo (TPN-USP) and Petrobras.

4.1 Metocean Data

The dataset of metocean information was observed from 2003 to 2009 and consists of 18006 different groups of environmental conditions with both unimodal and bimodal seas, defined by a total of up to 10 parameters by example: wind velocity and direction, current velocity and direction and up to 2 sets of wave related parameters.

As previously stated, in this paper only unimodal seas were considered, which are associated with just one set of parameters (H_s, T_p, β) to specify the sea state, and represent a total of over 5000 observations. The distribution of each of those parameters over the dataset is shown in Figs. 6, 7 and 8.

The histograms indicate the most common ranges of values for each of the parameters. As a result, the training of the neural networks may favor those values over the less frequent ones, given that some of those sets have considerably fewer examples than others. On the other hand, the models may learn to identify patterns related to the statistical description of waves of that geographical region.

In the case of the wave significant height, most occurrences are around 1.5 m to 2.5 m, while examples with height less than 1 m or greater than 4.5 m are rarely observed. Taking into account the wave peak periods, a substantial amount of waves with periods lower than $7 - 8$ s can be noticed, which correspond to high-frequency incident waves for a large vessel like the FPSO under analysis. This condition may be an issue for the estimation method, due to the already mentioned filtering problem. For the incidence directions, the most remarkable aspect is the almost absence of occurrences over 200°, which can be justified by

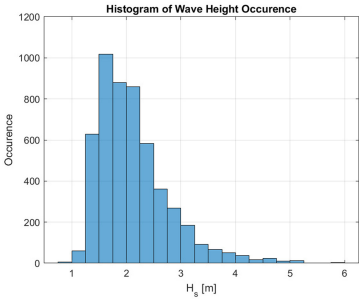

Fig. 6. Histogram of significant height

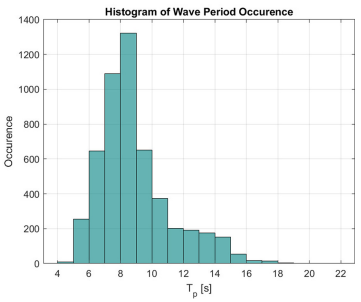

Fig. 7. Histogram of peak period

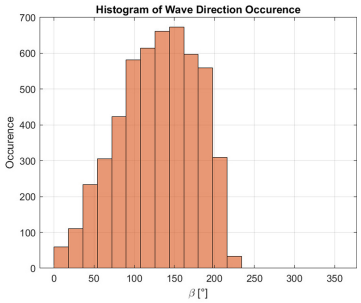

Fig. 8. Histogram of incidence direction

the geographical characteristic of the vessel's location. That is, waves with those incidence angles would be coming from the West, according to the polar plot of the directional spectrum in Fig. 3 (right), which would indicate waves coming from the Brazilian coast, and those situations are less frequent.

4.2 Data Processing

Before the actual training of estimators, a data treatment procedure was carried out on the time series obtained through the simulations. The output of the Dynasim simulator, for each set of conditions, is composed by time series of position, velocity and acceleration in the 6 dofs (surge, sway, heave, roll, pitch, yaw), which correspond to a time span of over 3 h (11400 s) with a sampling time of 1 s. From those series, just the 6 positional motions were selected, with respect to a fixed reference frame, and a time window of 30 min (1800 s), which is consistent with the regular dynamic of changes in the environment, was sampled in the middle of the total duration. Thereafter, each time series was centered by subtracting its mean value, and a dataset of over 5000 examples, each with 6 series of 1800 points, could be built.

The data was then divided into 3 different datasets, following a 70/20/10 split: the training data, to be used in the training of the network, the validation

data, used for the evaluation of the model with the desired metrics and the test data, to verify the performance of the system on previously unseen data. Finally, each dataset was normalized using the statistical properties (mean value and standard deviation) of the training dataset.

4.3 Network Architecture

In this paper, a single neural network architecture was sought to address, separately, the estimation problems of each of the sea state parameters. From the literature review, it was observed that the significant height estimation was more challenging than period and direction. Therefore, a sensitivity study with different classes of neural networks and their hyperparameters was run to select the network configuration with best performance, whose architecture would be then repeated to estimate peak period and incidence direction. In this way, the overall estimation was divided into 3 distinct problems, each with the same network structure trained independently with distinct targets.

A general structure for the pursued network was chosen as being composed of one or more feature extracting blocks (FE blocks) followed by a regression block. The latter was kept unchanged during the evaluations, while the former varied according to the following scenarios:

- MLP: Each FE block was built from multilayer perceptrons with batch normalization and ReLU activation functions. The number of layers (or blocks) was chosen from 1 to 3 and the number of neurons on each layer was selected from the set $\{64, 128, 256, 512\}$.
- LSTM: Each block was composed of LSTM layers with returning sequences. The number of layers varied from 2 to 4, and the number of units was picked from $\{32, 64, 128, 256, 512\}$.
- CNN1D - single kernel: 1D convolutional layers were employed, each convolution was followed by batch normalization and ReLU activation. The number of blocks was either 2 or 3, the number of filters was selected from $\{32, 64, 128, 256, 512\}$, and the kernel dimension of those filters from $\{1, 3, 5\}$.
- CNN1D - multiple kernels: This scenario was motivated by the structure proposed in Ref. [18], where convolutions with different kernels were combined to extract features in image classification. The number of layers was either 2 or 3, two sets of kernel dimensions were evaluated $\{1, 3, 5\}$ and $\{1, 3, 5, 7\}$ and the number of filters in the first layer was selected from $\{64, 128, 256, 512\}$, for the remaining layers the number of filters was half of the previous layer.
- CNN1D - multiple kernels with residual connections: Residual connections, inspired by Ref. [8], were added to the CNN1D with multiple kernels, where the input information was passed forward in the data flow.

In all scenarios, the regression block was the same, with 3 MLP layers—the first two with batch normalization and ReLU activation functions, and the last with a linear activation. The number of neurons in the layers was, respectively, 128, 64 and 1.

Table 2. Sensitivity study for network parameters

	& Layers	& Units/Filters	Filter kernel	Validation MAE [m]
MLP	2	[256, 256]	–	0.0608
LSTM	2	[512, 512]	–	0.1213
CNN1D - single kernel	2	[128, 128]	3	0.0442
CNN1D - multiple kernels	**2**	**[256,128]**	**{1,3,5,7}**	**0.0369**
CNN1D - multiple kernels and residual connections	2	[128, 64]	{1, 3, 5, 7}	0.0403

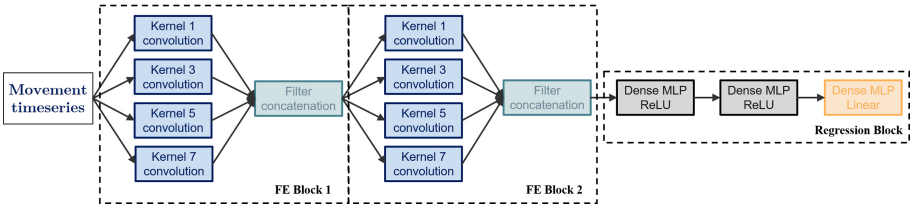

Fig. 9. Proposed network architecture

All experiments were carried out within a computational environment with Python 3.7.6. The layers were implemented by Keras 2.4.3, using TensorFlow 2.4.0 as the backend. The training process used the Adam optimizer, a batch size of 32 and a number of epochs of 1000. The selected loss function was the mean absolute error (MAE) between the actual significant wave height and the estimated one. The best model (based on the validation set) was stored during training.

The results of the sensitivity study are summarized in Table 2, where the best models obtained in each category, with respect to the validation MAE, along with their parameters, are presented.

From the analysis, it can be noted that the approaches based on convolutions presented a better performance compared to both MLP and LSTM. Furthermore, the association of filters with different kernels in a layer generated improvements, while the addition of residual connections did not bring benefits.

Those improvements can be justified by the definition of the convolutions, that were performed over windows of motions instead of time windows. The computations of each filter take into account all time samples and a number of movements equal to the kernel size; as a result, features related to the coupling of different combinations of motions can be extracted with multiple kernels. The proposed architecture is depicted in Fig. 9.

5 Motion-Based Estimation Results and Discussion

After selecting the network architecture through sensitivity analysis, the performance of the model was evaluated on the test dataset, with respect to the

Table 3. Comparison of wave height estimation results

	μ [m]	σ [m]	MAE [m]	$MAPE$ [%]	R^2
Proposed	0.0007	0.0644	0.0384	1.9087	0.9903
SSENET (adapted from [3])	0.0000	0.1071	0.0675	3.3505	0.9733
MLSTM-CNN [6]	0.0063	0.0953	0.0561	2.6868	0.9788
Sliding Puzzle [6]	−0.0002	0.0633	0.0400	1.9191	0.9907

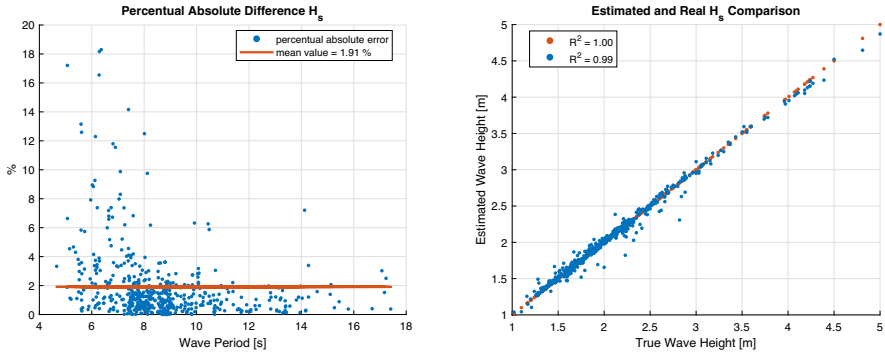

Fig. 10. Regression results - wave height

following metrics: mean value (μ) and standard deviation (σ) of the error, mean absolute error (MAE), mean absolute percentual error ($MAPE$), and the coefficient of determination (R^2).

Moreover, the results attained by the proposed architecture were compared to other neural networks available in the literature for sea state estimation, that were implemented and trained with the same dataset. In particular, three networks were employed: SSENET, from Ref. [3], based on convolutions with residual connections; MLSTM-CNN, from Ref. [6], combining CNN and LSTM layers; and Sliding Puzzle, also from Ref. [6], with a purely convolutional architecture. Although the SSENET was designed for a classification task, its structure was adapted for the considered regression problem, which may provide illustrative results for comparison purposes. The MLSTM-CNN and the Sliding Puzzle remained unchanged since they were already designed for regression.

The summary of the results for the wave height estimation is presented in Table 3. There it can be observed that, except for mean value of the error, the architectures built only with convolutional layers (Proposed and Sliding Puzzle) presented a better performance when compared to the others, with a slightly better result of the Proposed in the MAE and MAPE, and slightly worse on the standard deviation and R^2. It is also worth pointing out that in both cases the average errors were low, with less than 2% error, 0.04 m of absolute error, and the R^2 was over 0.99.

Table 4. Comparison of wave period estimation results

	μ [s]	σ [s]	MAE [s]	$MAPE$ [%]	R^2
Proposed	–0.0063	0.1074	0.0553	0.7210	0.9977
SSENET (adapted from [3])	–0.0060	0.0903	0.0552	0.7215	0.9984
MLSTM-CNN [6]	0.0017	0.0691	0.0446	0.5742	0.9990
Sliding Puzzle [6]	−0.0040	0.0471	0.0283	0.3653	0.9996

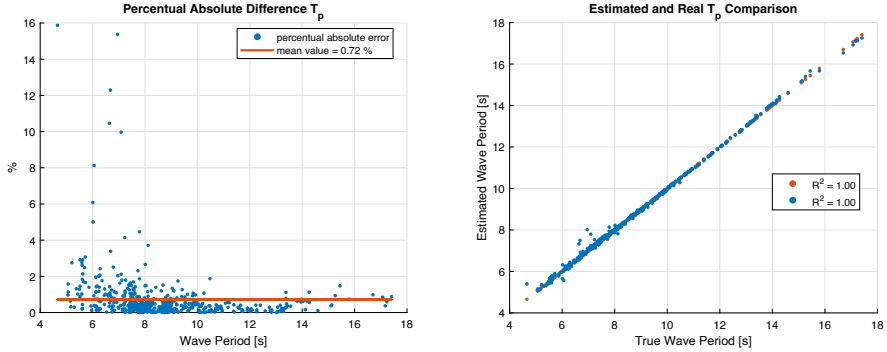

Fig. 11. Regression results - wave period

A further analysis is enabled by the (percentage) absolute difference plot and the comparison between actual and estimated values in Fig. 10.

From these plots, two main effects can be outlined: the filtering problem, given that the largest errors occurred at the low periods, and that true and estimated values on high height values, over 4 m, did not present large differences, despite few occurrences.

Similarly, for the peak period, the comparative results are shown in Table 4. From there it can be verified that all the architectures are able to present significant results, less than 0.8% of percentual error, and no more than 0.06 s of absolute error on average. However, for this sea state parameter, the proposed network was outperformed by the other approaches.

The plots in Fig. 11 show the same tendency of the height estimation: presence of filtering affecting the performance in low periods, and even though few examples with high periods are available, their estimation had small errors.

For the incidence direction, some differences from the previous cases are worth discussing. Given the circular characteristics of the target, a custom loss function was adapted considering the distance of two points (P_1, P_2) in the unitary circle with angular coordinates β_1 (true value) and β_2 (estimation), which is stated as:

$$d(P_1, P_2) = \sqrt{(\sin\beta_1 - \sin\beta_2)^2 + (\cos\beta_1 - \cos\beta_2)^2}. \tag{3}$$

Table 5. Comparison of wave direction estimation results

	μ [°]	σ [°]	MAE [°]	R^2
Proposed	–0.1427	1.4533	0.5661	0.9991
SSENET (adapted from [3])	–0.0099	3.4532	0.8689	0.9951
MLSTM-CNN [6]	–0.0458	2.8728	1.3340	0.9969
Sliding Puzzle [6]	–0.2411	3.8300	1.2278	0.9939

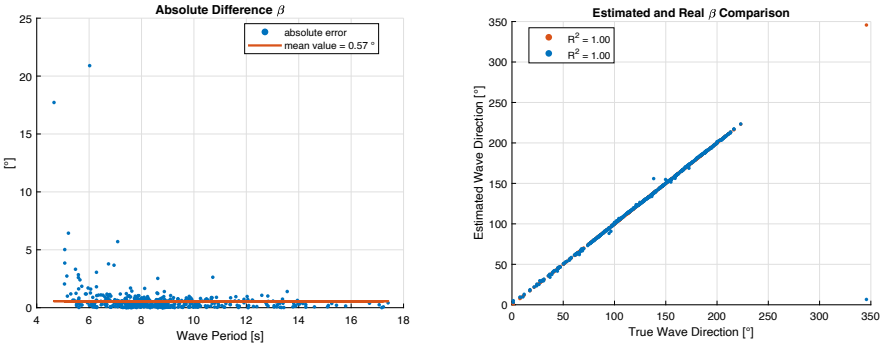

Fig. 12. Regression results - wave direction

And then, the absolute angular difference in the range $[0, \pi]$ can be obtained with the cosine law:

$$d(P_1, P_2)^2 = 1^2 + 1^2 - 2cos(\beta_1 - \beta_2) \Rightarrow |\beta_1 - \beta_2| = \arccos\left(1 - \frac{d(P_1, P_2)^2}{2}\right). \quad (4)$$

From the expression, it can be noted that the absolute angular error increases if $d(P_1, P_2)$ increases. Thus, the loss function was defined as the distance itself, in order to avoid computations of derivatives of the inverse cosine function.

The results of the direction estimation are shown in Table 5. As in the previous cases, the error metrics displayed low values in all methods—less than 1.5° in the MAE, for example. But for most of the metrics, except the mean value of the error, the proposed model generated better outcomes than other methods.

The plots in Fig. 12 highlight once again the difficulty in the estimation at low periods, with large deviations from the mean in those situations. And also the limited number of directions over 200°, which could still be properly estimated.

Overall, the proposed architecture produced significant results in the sea state estimation based on motions of a moored FPSO obtained through simulations; low errors metrics were attained and even less frequently observed parameters could be estimated. The well-known filtering problem was also observed in all evaluations. However, in most cases, either the errors in the high-frequency range were acceptable, less than 19% for height and period, or the number of occurrences with large deviations was very restricted, just 2 cases over 7° of absolute

error in the direction. This may suggest that patterns were extracted from data related to the movement generated by those high-frequency waves, which may have led the network to use information not only from the first-order response but also from the slow varying motions (due to higher-order wave-induced effects) in the inference; or that the models were able to learn about the statistical distribution of the dataset of environmental conditions of the region—or some other feature that requires further analysis in the continuation of the work.

6 Conclusions

A supervised learning approach for motion-based sea state estimation with neural networks has been presented in this paper. Time series of movements, generated through simulations of a spread-moored FPSO with constant draft under environmental conditions observed at Brazil's Campos Basin, were applied to train the networks so as to estimate each of the sea state parameters. A single network architecture was obtained from a sensitivity study run on different classes of neural networks and their hyperparameters, based on the significant height estimation. Convolutional layers with multiple kernels concatenated were selected, allowing us to analyze coupling of motions among different sets of dofs.

Results obtained by the proposed architecture were compared to other networks designed for sea state estimation available in the literature and presented comparable or slightly better performance in the evaluated error metrics. The examination of the estimation outcomes in the individual examples displayed the classical filtering problem, in which high-frequency waves are filtered by the vessel. Despite that, the performance loss, although significant, did not completely compromise the estimation, which may lead one to question whether or not the network is able to extract features related to those settings—by the slow varying information present in the time series, by learning patterns of the statistical distribution of the environmental conditions of the region, or by some other aspect. Those circumstances motivate further developments on the work; for instance, the analysis for bimodal seas and multiple loading conditions, and the continuous search for possibly more suitable estimation models.

Acknowledgments. Authors acknowledge Petrobras for providing long-term support and motivation to this work. The authors also thank the Center for Artificial Intelligence (C4AI-USP) and the support from the São Paulo Research Foundation (FAPESP grant #2019/07665-4) and from the IBM Corporation. The first and second authors acknowledge the Higher Education Personnel Improvement Coordination (Capes) for the scholarship. The third author was supported in part by Brazilian National Council for Scientific and Technological Development (CNPq) under Grant 312180/2018-7. The last author acknowledges the CNPq for the research grant (310127/2020-3).

References

1. Arneson, I.B., Brodtkorb, A.H., Sørensen, A.J.: Sea state estimation using quadratic discriminant analysis and partial least squares regression. IFAC-PapersOnLine **52**(21), 72–77 (2019)

2. Brodtkorb, A.H., Nielsen, U.D., Sørensen, A.J.: Sea state estimation using vessel response in dynamic positioning. Appl. Ocean Res. **70**, 76–86 (2018)
3. Cheng, X., Li, G., Ellefsen, A.L., Chen, S., Hildre, H.P., Zhang, H.: A novel densely connected convolutional neural network for sea-state estimation using ship motion data. IEEE Trans. Instrum. Meas. **69**(9), 5984–5993 (2020)
4. Da Silva Bispo, I.B., Simos, A.N., Tannuri, E.A., da Cruz, J.J., et al.: Motion-based wave estimation by a Bayesian inference method: a procedure for pre-defining the hyperparameters. In: The Twenty-second International Offshore and Polar Engineering Conference. International Society of Offshore and Polar Engineers (2012)
5. De Souza, F.L., Tannuri, E.A., de Mello, P.C., Franzini, G., Mas-Soler, J., Simos, A.N.: Bayesian estimation of directional wave-spectrum using vessel motions and wave-probes: proposal and preliminary experimental validation. J. Offshore Mech. Arctic Eng. **140**(4), 041102 (2018). https://doi.org/10.1115/1.4039263. ISSN 0892-7219
6. Duz, B., Mak, B., Hageman, R., Grasso, N.: Real time estimation of local wave characteristics from ship motions using artificial neural networks. In: Okada, T., Suzuki, K., Kawamura, Y. (eds.) PRADS 2019. LNCE, vol. 65, pp. 657–678. Springer, Singapore (2021). https://doi.org/10.1007/978-981-15-4680-8_45
7. Goodfellow, I., Courville, A., Bengio, Y.: Deep Learning, vol. 1. MIT Press, Cambridge (2016)
8. He, K., Zhang, X., Ren, S., Sun, J.: Deep residual learning for image recognition. In: Proceedings of the IEEE Conference on Computer Vision and Pattern Recognition, pp. 770–778 (2016)
9. Hochreiter, S., Schmidhuber, J.: Long short-term memory. Neural Comput. **9**(8), 1735–1780 (1997)
10. Journée, J.M., Massie, W.W.: Offshore Hydromechanics. Delft University of Technology, Delft, The Netherlands (2001)
11. LeCun, Y., Bengio, Y., et al.: Convolutional networks for images, speech, and time series. Handb. Brain Theor. Neural Netw. **3361**(10), 1995 (1995)
12. Ma, K.T., Luo, Y., Kwan, C.T.T., Wu, Y.: Mooring System Engineering for Offshore Structures. Gulf Professional Publishing, Houston (2019)
13. Newman, J.N.: Marine Hydrodynamics. The MIT press, Cambridge (1977)
14. Nielsen, U.D.: Estimations of on-site directional wave spectra from measured ship responses. Mar. Struct. **19**(1), 33–69 (2006)
15. Pecher, A., Kofoed, J.P. (eds.): Handbook of Ocean Wave Energy. OEO, vol. 7. Springer, Cham (2017). https://doi.org/10.1007/978-3-319-39889-1
16. Simos, A.N., Tannuri, E.A., da Cruz, J.J., Filho, A.N.Q., Da Silva Bispo, I.B., Carvalho, R.C.: Development of an on-board wave estimation system based on the motions of a moored FPSO: Commissioning and preliminary validation. In: International Conference on Offshore Mechanics and Arctic Engineering, vol. 44922, pp. 259–270. American Society of Mechanical Engineers (2012)
17. Simos, A.N., Tannuri, E.A., Sparano, J.V., Matos, V.L.: Estimating wave spectra from the motions of moored vessels: experimental validation. Appl. Ocean Res. **32**(2), 191–208 (2010)
18. Szegedy, C., et al.: Going deeper with convolutions. In: Proceedings of the IEEE Conference on Computer Vision and Pattern Recognition, pp. 1–9 (2014)
19. Tannuri, E.A., Sparano, J.V., Simos, A.N., Da Cruz, J.J.: Estimating directional wave spectrum based on stationary ship motion measurements. Appl. Ocean Res. **25**(5), 243–261 (2003)
20. Tu, F., Ge, S.S., Choo, Y.S., Hang, C.C.: Sea state identification based on vessel motion response learning via multi-layer classifiers. Ocean Eng. **147**, 318–332 (2018)